Role of molecular oxygen and other impurities in the electrical transport and dielectric properties of C_{60} films

B. Pevzner
Department of Electrical Engineering and Computer Science, Massachusetts Institute of Technology, Cambridge, Massachusetts 02139

A. F. Hebard*
Bell Laboratories, Lucent Technologies, Murray Hill, New Jersey 07974

M. S. Dresselhaus
Department of Electrical Engineering and Computer Science and Department of Physics, Massachusetts Institute of Technology, Cambridge, Massachusetts 02139

(Received 10 June 1996; revised manuscript received 3 March 1997)

We have used dielectric spectroscopy to measure the frequency and temperature dependence of the low-frequency (0.5 mHz–100 kHz) complex dielectric function $\varepsilon(\omega)$ of thin C_{60} films. A small charge transfer occurs between the C_{60} and O_2 molecules which occupy interstitial spaces of solid C_{60} exposed to oxygen (or ambient air). Due to the large size of the C_{60} molecules, this small charge transfer creates large dipole moments, which in turn are coupled to the applied ac electric field via a *diffusion-controlled relaxation* mechanism. This gives rise to a significant increase in the permittivity ε_1 accompanied by a broad dielectric loss peak ε_2 observed at $\sim$10–100 Hz. With increasing oxygenation, the interstitial sites become nearly fully occupied, interstitial hopping is inhibited, and the loss peaks, together with the enhanced polarization, disappear. Both tracer and chemical diffusion coefficients for the C_{60}/O_2 system have been obtained purely from dielectric spectroscopy measurements. [S0163-1829(97)05423-4]

I. INTRODUCTION

Since the discovery by Krätschmer *et al.*[1] of the method for bulk synthesis of fullerene C_{60}, the complex dielectric function $\varepsilon(\omega)=\varepsilon_1(\omega)+i\varepsilon_2(\omega)$ of solid C_{60} films was studied over a broad frequency range using a wide variety of techniques.[2–7] The optical dielectric function $\varepsilon(\omega)$ of C_{60} was mapped out in the range of 10^{13}–10^{16} Hz (corresponding to 0.05–40 eV) using infrared, vis-UV, and electron-energy-loss spectroscopies.[8] Figure 1 presents a summary of experimental data reported for the real $\varepsilon_1(\omega)$ and imaginary $\varepsilon_2(\omega)$ parts of the dielectric function at 300 K over the entire optical frequency range from the infrared through the ultraviolet.

While the features of the C_{60} optical spectrum have been described in considerable detail elsewhere,[8] we note here the general trend that, as we move toward lower and lower frequencies, for every loss process represented by a peak in the dielectric loss $\varepsilon_2(\omega)$, there is a rise (sometimes predicated by a resonant oscillation) in $\varepsilon_1(\omega)$, as prescribed by the Kramers-Kronig relations. At frequencies below 10^{13} Hz, the dielectric function incorporates all electronic and vibrational (phonons) contributions, and so $\varepsilon_1(\omega)$ is approaching its dc value. The small difference between $\varepsilon_1(10^{13}\ \text{Hz})\approx 3.9$ (Ref. 5) and $\varepsilon_1(10^5\ \text{Hz})\approx 4.4$ (Ref. 2), shown by an arrow in Fig. 1, might be due to the losses associated with C_{60} molecules rapidly rotating above the structural phase transition temperature $T_{01}=260$ K at the rate of $\sim 10^9$ Hz, as shown by NMR,[9] ultrasound attenuation,[10] and other experiments sensitive to phenomena in this frequency range.

From the Kramers-Kronig relations, it follows, for the case of zero frequency,

$$\varepsilon_1(0)-1=\frac{2}{\pi}\int_0^\infty \frac{\varepsilon_2(\omega)}{\omega}d\omega=\frac{2}{\pi}\int_0^\infty \varepsilon_2(\omega)d(\ln\omega), \quad (1)$$

telling us that the dc dielectric constant $\varepsilon_1(0)$ includes *all* contributions from the higher-frequency loss processes, and is proportional to the area under the $\varepsilon_2(\omega)$ curve plotted on a logarithmic scale.[11] In this paper, we report measurements of the dielectric function $\varepsilon(\omega)$ of C_{60} thin films for frequencies *below* 10^5 Hz, where polarization mechanisms come into play.

After a brief overview of experimental details (Sec. II), evidence for oxygen diffusion into fullerene solids is presented in Sec. III. Section IV demonstrates how a small charge transfer occurring between the C_{60} and O_2 molecules occupying interstitial spaces of solid C_{60} creates large dipole moments, which are coupled to the applied ac electric field via a *diffusion-controlled relaxation* mechanism. This gives rise to a significant increase in the observed permittivity ε_1 at low frequencies ($\sim$10–100 Hz) accompanied by a broad dielectric loss peak ε_2. With increasing oxygenation, the interstitial sites become nearly fully occupied, interstitial hopping is inhibited, and the loss peaks, together with the enhanced polarization, disappear. The temperature-dependent behavior of the dielectric function $\varepsilon(\omega)$ of C_{60} films is presented in Sec. V, followed by conclusions (Sec. VI).

II. EXPERIMENTAL DETAILS

All samples used in this study were prepared at Bell Laboratories (Murray Hill, NJ). For thin-film deposition, 10–15 mg of 99.9% purified C_{60} powder were loaded into alumina crucibles. The rotating substrate (either at ambient

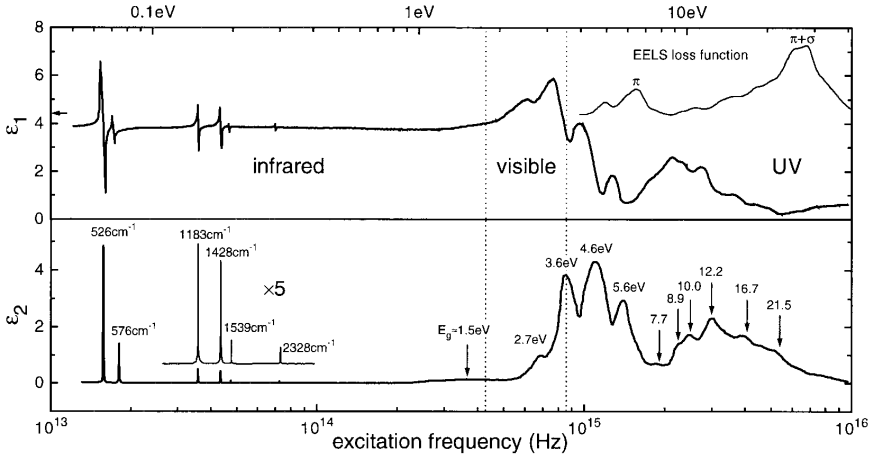

FIG. 1. Summary of real $\varepsilon_1(\omega)$ and imaginary $\varepsilon_2(\omega)$ parts of the dielectric function for C_{60} vacuum-sublimed solid films at room temperature over a wide frequency range. The data between 0.05 and 0.5 eV (mid- to near-infrared) were collected using the Fourier transform infrared (FTIR) transmission technique (Ref. 6). The vis-UV range was investigated by variable angle spectroscopic ellipsometry (VASE) (Ref. 4), and near-normal-incidence reflection and transmission experiments (Ref. 5). UV data above ~ 7 eV were obtained using electron-energy-loss spectroscopy (EELS) (Ref. 7) by Kramers-Kronig analysis of the EELS loss function (inset). The arrow at the left axis points to $\varepsilon_1 = 4.4$, the observed low frequency value of the dielectric constant (Ref. 2).

or at elevated temperature, up to $\sim 200\,^{\circ}$C), was located approximately 10 cm from the crucibles, and a quartz-crystal microbalance was used to monitor the rate of deposition and final film thickness. Quartz, fused quartz, and glass (Pyrex) substrates were used for most of the transport and dielectric experiments. The details of the film deposition procedure are presented elsewhere.[2,12]

After deposition, the thickness of the films was determined by ellipsometry (or by profilometry, for thicker films), and was generally found to be in good agreement with the readings of the calibrated thickness monitor. UV-vis and Raman spectroscopy, x-ray powder diffraction, and high-resolution transmission electron microscopy were used to ascertain the fcc structure and to characterize the morphology of the films.[12] Small crystallites on the order of 100 Å in diameter were typical. In order to assess the oxygen content of our films, electron-spin resonance and weight uptake techniques were used.

To investigate the electrical properties of the C_{60} films, we fabricated Al-C_{60}-Al trilayer structures for electrical characterization (Fig. 2). These ''sandwich'' structures were made by depositing in succession, on glass, 200-μm-wide aluminum down stripes, a known thickness of C_{60}, and finally, 200-μm-wide aluminum cross stripes. We used these trilayer devices to measure the intrinsic (static) dielectric constant of C_{60} films.

In order to ascertain the intrinsic dc $\varepsilon_1(0)$ of C_{60}, the dielectric measurement needs to be performed at frequencies low enough to include the intrinsic relaxation processes of the material, but high enough to escape the effect of impurities (e.g., molecular oxygen). We have determined experimentally that the effects of oxygen and other impurities occupying the interstitial sites of solid C_{60} on the dielectric relaxation of C_{60} films are confined to frequencies below ~ 5 kHz. The intrinsic dielectric constant was obtained by performing a series of capacitance measurements at 100 kHz on trilayer structures, similar to the one shown in Fig. 2, where the thickness of the C_{60} layer was varied from 200 to 1000 Å.[2] From the slope of the measured linear dependence of the reciprocal capacitance on the film thickness, a value $\varepsilon_1 = 4.4 \pm 0.2$ for the relative dielectric constant was obtained.[2]

A coplanar electrode configuration was used as an alternative to the ''sandwich'' configuration for some dielectric and transport measurements. This geometry (see Fig. 3) is often preferable to the ''sandwich'' geometry, because (1) the comb electrodes of a coplanar sensor ensure proper calibration of the device even if the material being measured

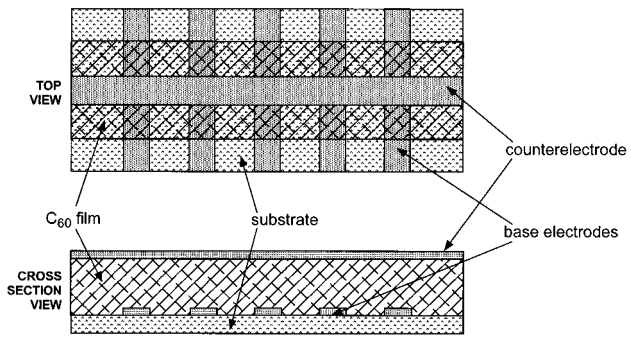

FIG. 2. A typical trilayer (''sandwich'') structure is composed of five identical Al-C_{60}-Al junctions, each of which can be used independently in a dielectric (or transport) experiment.

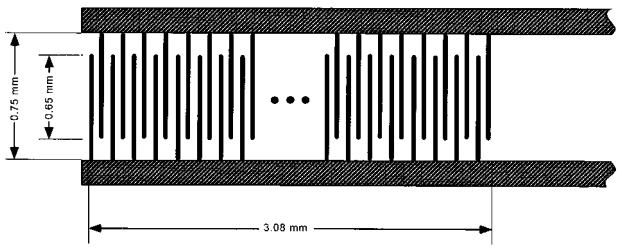

FIG. 3. The coplanar sensor geometry. Chromium electrodes (1500 Å thick) deposited on a quartz substrate are configured to provide a 1 μm interelectrode spacing and a 1 m meander length.

undergoes structural transformations (e.g., structural phase transitions, such as that experienced by C_{60} at $T_{01}=260$ K), and (2) the open-face layout facilitates studies of diffusion of foreign species into the bulk of the material.

Depending on the design details of the coplanar sensor, it can be utilized either for dielectric or for transport measurements. The former use, giving rise to a technique known as *microdielectrometry*,[13–15] has been employed to study the effects of various treatments on the dielectric properties of the C_{60} films, and the results thus obtained will be discussed in future work. In the present study, we used such coplanar sensors, comprising 1-μm-spaced interdigitated chromium electrodes patterned on a quartz substrate, for transport measurements. In this use, a C_{60} film of known thickness was deposited directly onto the surface of the sensor.

The ac dielectric measurements were performed using a Hewlett-Packard HP 4274A LCZ Meter for frequencies from 100 Hz to 100 kHz, and a Solartron Instruments SI 1254 Frequency Response Analyzer cascaded with a Stanford Research SR 570 current amplifier for frequencies from 1 mHz to 1 kHz.

III. OXYGEN DIFFUSION INTO FULLERENE SOLIDS

Since oxygen has proved to be one of the most important intercalants affecting the electrical properties of C_{60} films, it is worthwhile to discuss the evidence for oxygen intercalation into the bulk of solid C_{60} in more detail. Unlike alkali-metal intercalants, which can transfer a large amount of charge (one electron per alkali-metal atom) to the C_{60} balls, a very low charge transfer occurs for the case of oxygen intercalation. This charge transfer gives rise to the enhanced polarization effects described in Sec. IV, where it is shown that the amount of charge transferred by oxygen molecules is between 20 and 100 times less than that transferred by alkali-metal atoms.

A variety of experiments provide evidence for oxygen diffusion in fullerites. Assink *et al.*[16] used ^{13}C NMR spectroscopy to show that molecular oxygen diffuses readily into the octahedral interstitial sites of the fcc lattice of C_{60}. Eloi *et al.*[17] verified the increase in the diffusion rate of O_2 into the fcc C_{60} lattice under UV irradiation by direct measurement of the oxygen uptake via resonant α-particle scattering experiments.

Given the exponential dependence of the conductivity on the position of the Fermi level in a semiconductor, conductivity measurements can provide an extremely sensitive way of monitoring the density of electronic states in the band gap or near the band edges of crystalline C_{60} caused by oxygen, light, or other perturbations. In particular, oxygen decreases the intrinsic conductivity of fullerites by as much as four orders of magnitude. The magnitude of this effect, together with the propensity for solid C_{60} to adsorb oxygen from the surrounding atmosphere, is responsible for the unusually wide (up to ten orders of magnitude) dispersion in the values for the conductivity of C_{60} reported in the literature[18–29] (see Fig. 4).

To characterize the conductivity (and, by inference, the oxygen content) of our C_{60} films, we have performed transport measurements using the coplanar sensor (Fig. 3). Typically, a 2000-Å-thick C_{60} film was deposited on the sensor as described in Sec. II, and its conductivity was measured for temperatures ranging from 25 to 250 °C, as shown in Fig. 5.

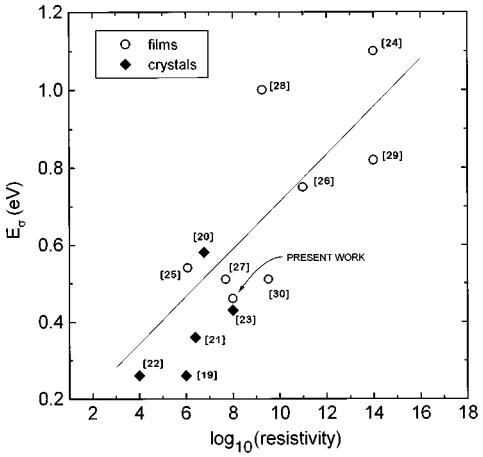

FIG. 4. Room-temperature resistivity $\rho=1/\sigma$ (Ω cm) and activation energy E_σ values reported for C_{60} single crystals and highly crystalline films (solid diamonds), and for polycrystalline and amorphous C_{60} films (open circles) (Ref. 18–29). E_σ is the activation energy for temperatures above the structural transition $T_{01}=260$ K. The straight line through the data is the result of a linear regression analysis.

It is immediately evident from the data in Fig. 5 that annealing increases the conductivity of C_{60} films, probably both by improving the crystallinity of the film and by driving oxygen out of the interstitial regions. The kink in the curve at $T\approx 120$ °C during the temperature up-sweep probably corresponds to the onset of oxygen effusion. Region 1 of the curve thus corresponds to the oxygen-filled C_{60}, which has a conductivity exhibiting an activation energy of $E_\sigma=0.44$ eV. Above $T\approx 120$ °C (region 2 of the curve), oxygen is expelled out of the C_{60} solid. This process is also activated in temperature, and it affects the conductivity of the film. Thus

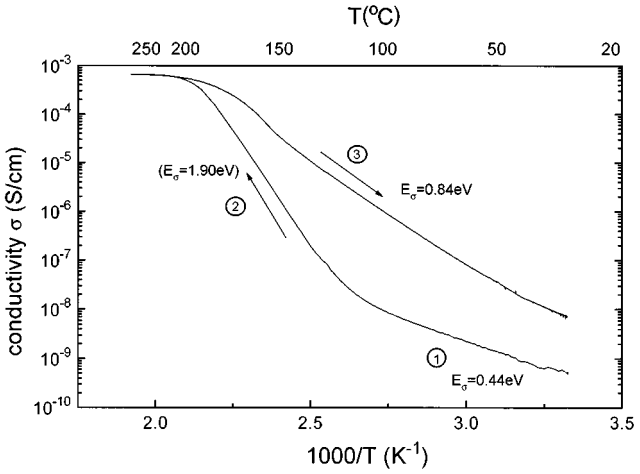

FIG. 5. Transport measurements of a C_{60} film. The measured conductivity of C_{60} (log scale) is plotted vs $1000/T$ on an Arrhenius plot. Arrows indicate the direction of the temperature scan, and the circled numbers indicate temperature regions corresponding to the indicated E_σ values. The measurements were performed using the coplanar sensor at an applied voltage level of 1 V. The average temperature scanning rate was ~ 0.2 °C/min.

the activation energy of the effusion adds to the activation energy of oxygenated C_{60}, yielding a relatively high (relative to the optical absorption edge) value $E_\sigma = 1.90$ eV. Since oxygen molecules leaving the C_{60} film no longer participate in the C_{60} transport (e.g., as carrier traps), the value $E_\sigma = 1.90$ eV for the combined activation energy of transport and effusion has no straightforward interpretation.

The curve in Fig. 5 levels off at $\sim 220\,^\circ$C, as C_{60} molecules start to sublimate from the substrate (a first-order phase transition). Region 3 of the curve in Fig. 5, subsequent to annealing, where the conductivity is activated by $E_\sigma = 0.84$ eV, corresponds to the rapid adsorption of oxygen by the deoxygenated C_{60}. Since this is a transient process, no reliable determination of the intrinsic activation energy of C_{60} can be made from these data.

Note that the summary of C_{60} conductivity studies shown in Fig. 4 suggests that the amount of adsorbed oxygen played a large role in many of the reported σ and E_σ studies. Authors reporting lower conductivities for C_{60} films and crystals also tend to report higher activation energies, and vice versa. This can be explained by observing that, when introduced into the interstitials of a fullerene material, molecular oxygen quenches the conductivity and creates deep electronic traps. The more oxygen present in the C_{60} matrix, the deeper these traps are, and thus the higher the activation energy is. Our study shows reversibility of oxygen diffusion with annealing,[16,21] and provides an explanation for the wide range of values reported in the literature for the room temperature conductivity and the corresponding activation energy (Fig. 4).

When analyzed together, this work and previously reported studies of C_{60} transport strongly suggest that oxygen affects the transport properties of the C_{60} films in at least two distinct ways. In the first few minutes of exposure, oxygen diffuses through the intergrain boundaries, rapidly quenching electronic transport, and decreasing the intrinsic conductivity of C_{60} by one or two orders of magnitude. Then, in a slow process that can run for hours or even days, oxygen diffuses into the interstitial spaces of the fullerite crystallites, lowering the conductivity of the material by about two more orders of magnitude. Additional evidence supporting this proposition is provided by our studies of low-frequency dielectric properties of fullerene thin films reported below.

IV. DIELECTRIC PROPERTIES AS A FUNCTION OF OXYGEN DIFFUSION

The interstitial spaces of the fcc C_{60} solid are large enough to accommodate almost any element of the Periodic Table. In this section, we shall investigate how molecular oxygen affects the dielectric properties of C_{60} films. First, we describe the development and dynamics of a low-frequency dielectric loss peak (accompanied by an increase in polarization) with prolonged exposure to ambient oxygen (Sec. IV A). In Sec. IV B, we hypothesize that these impurities consist mainly of molecular oxygen, and then demonstrate that very little charge transfer is necessary in order to achieve the polarization enhancements reported in Sec. IV A, which makes the oxygen diffusion model of dielectric relaxation in oxygenated C_{60} highly plausible. In Sec. IV C, we propose a *diffusion-controlled relaxation* model for low-frequency dielectric relaxation of oxygenated C_{60}, which explains the dynamics of the dielectric loss peak as a function of oxygen content. Finally, Sec. IV D describes how to obtain both tracer and chemical diffusion constants for oxygen diffusion into C_{60} purely from dielectric measurements.

A. Development of dielectric loss peaks through oxygen diffusion

The presence of electric dipoles in oxygenated solid C_{60} is further confirmed by dielectric studies of C_{60} thin films using the trilayer sample configuration (Fig. 2). The main feature consistently appearing in the dielectric measurements of all C_{60} films we have studied is a significant increase in permittivity ε_1 as the frequency is decreased, accompanied by a peak in the dielectric loss ε_2, at frequencies on the order of 10–1000 Hz at room temperature. These features are dependent on both the concentration of oxygen in the interstitials of the film and on temperature. These relationships are discussed here and in Sec. V, respectively.

Figure 6 displays a representative ''snapshot'' of the real and imaginary parts of the dielectric function of a 1000-Å C_{60} film after 16 h of exposure to the ambient environment at room temperature ($T \approx 296$ K). The figure shows the frequency dependence of the real (a) and imaginary (b) parts of the dielectric function, as well as the loss tangent (c). The data for the C_{60} film (solid lines) are compared to the Debye single-relaxation-time model described by the following equations for permittivity and dielectric loss:

$$\varepsilon_1(\omega) = \varepsilon_\infty + \frac{\varepsilon(0) - \varepsilon_\infty}{1 + (\omega\tau_d)^2} \tag{2}$$

$$\varepsilon_2(\omega) = [\varepsilon(0) - \varepsilon_\infty]\frac{\omega\tau_d}{1 + (\omega\tau_d)^2} \tag{3}$$

where $\omega = 2\pi f$ is the angular frequency, $\varepsilon_\infty \approx 4.4$ is the intrinsic permittivity of C_{60} (see Sec. II), $\varepsilon(0)$ is the static permittivity incorporating the effect of additional polarization mechanisms to be discussed in Sec. IV B, and τ_d is the relaxation time parameter. The frequency dependence of the loss tangent D for a simple case of parallel-plate measurements is given by

$$D(\omega) = \frac{\varepsilon_2(\omega)}{\varepsilon_1(\omega)} + \frac{d}{\omega\varepsilon_0\varepsilon_1(\omega)AR_0}, \tag{4}$$

where A is the cross-sectional area of the capacitor, d is the separation between the plates (Fig. 2), R_0 is the dc resistance of the sample, and ε_0 is the permittivity of free space.

We immediately notice that our system cannot be adequately described by a simple Debye relaxation mechanism, or, for that matter, any of the other popular single-parameter models (Cole-Cole, Davidson-Cole, or Williams-Watts).[11,12] However, the data can easily be fit to a two-parameter relaxation model, such as the universal relaxation model proposed by Jonscher,[11] in which the dielectric loss may be represented by the empirical law combining two power laws, respectively, below and above the peak frequency ω_p,

$$\varepsilon_2(\omega) \sim \frac{1}{(\omega/\omega_p)^{-m} + (\omega/\omega_p)^{1-n}}, \tag{5}$$

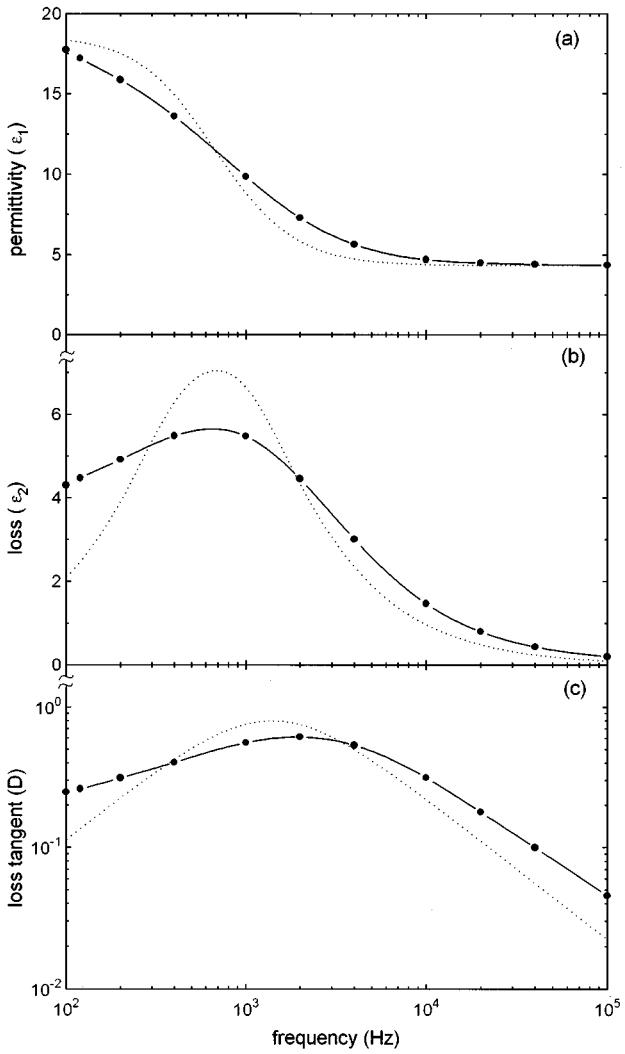

FIG. 6. Dielectric response of a 1000-Å-thick C_{60} film after 16 h of exposure to the ambient environment at room temperature ($T \approx 296$ K). The real (a) and imaginary (b) parts of the dielectric function are plotted vs frequency f on a log-linear scale, whereas the loss tangent (c) is shown on a log-log scale. The dotted lines correspond to the best fit to the Debye relaxation function [Eqs. (2) and (3)] with the following parameters: $\varepsilon_\infty = 4.4$, $\varepsilon(0) = 18.7$, $f_{\text{peak}} = 674$ Hz, and $\tau_d = 1/2\pi f_{\text{peak}} = 236$ μs.

where the exponents m and $1-n$ fall in the range (0,1) and the peak frequency ω_p is generally temperature dependent. The linear fits to the log-log plot of the loss tangent data in Fig. 6(c) suggest the high- and low-frequency exponents of 0.87 and 0.19, respectively. These exponents are dependent on both temperature and oxygen content of the C_{60} film, and vary slightly from one sample to another.

As oxygen diffuses into the bulk of the C_{60} films, the dielectric loss peaks change their magnitude, shape, and frequency position. Figure 7 schematically illustrates the dynamics of the loss peak as a function of exposure to ambient oxygen. The curve after 1 h of exposure in Figs. 7(a) and 7(b) shows that as-prepared films display very little anomalous dielectric dispersion, resulting in the absence of the dielectric loss peak. The $1/f$ rise in the dielectric loss tangent toward low frequencies is due to the finite dc conductivity of the sample. With prolonged exposure to oxygen, the loss tangent peak in Fig. 7(b) becomes more pronounced, and gradually moves toward higher frequencies by about an order of magnitude in the trace taken after 116 h. With additional exposure, however, the dielectric loss peak decreases again, until the peak finally disappears completely after about two weeks of exposure to ambient conditions. It should be noted that, after a 10-h heat treatment in vacuum ($T_{\text{HT}} \simeq 200$ °C), the dielectric peak is recovered, with its position suggesting that some residual oxygen is still left in the bulk of the film.

B. Impurity-induced polarization

The development of the dielectric peaks, such as the one shown in Fig. 6(b), after oxygen exposure provides further evidence for the presence of dipoles in oxygenated C_{60} films. The fact that both C_{60} and oxygen (O_2) molecules are nonpolar, together with the evidence of reversible oxygen diffusion into the bulk of solid C_{60} (Sec. IV A), strongly suggest that these dipoles arise from charge transfer between oxygen molecules and C_{60} balls. On the other hand, the amount of this charge transfer is bound to be very small, reflecting the fact that the electron affinities of both C_{60} and molecular oxygen are relatively high. The direction of the charge transfer can be ascertained by comparing the electron affinities of these two molecules. Since the electron affinity of the C_{60} molecule [2.65 ± 0.05 eV (Ref. 8)] is considerably higher than that of molecular oxygen [0.451 ± 0.007 eV (Ref. 30)], one might expect oxygen to be the donor and C_{60} the acceptor of electrons.

Even though the amount of charge transferred from an oxygen molecule to a C_{60} molecule may be small, it can create a relatively large effective dipole moment if the charge is transferred over a large distance. To calculate the amount of charge that needs to be transferred in order to achieve the added polarization evident in Fig. 6(a), we shall use the Clausius-Mossotti equation[11] relating the relative permittivity ε_1 of a solid to the dipole moment μ of the permanent dipoles contained in the solid and to the molecular polarizability α_m,

$$\frac{\varepsilon_1 - 1}{\varepsilon_1 + 2} = \frac{N_d \mu^2}{9\varepsilon_0 k_B T} + \frac{4\pi N_m \alpha_m}{3}, \tag{6}$$

where N_m is molecular density of the solid, N_d is the density of permanent dipoles, and the fundamental constants are $\varepsilon_0 = 8.85 \times 10^{-12}$ F/m and $k_B = 1.38 \times 10^{-23}$ J/K, the permittivity of free space, and the Boltzmann constant, respectively. In the absence of permanent dipoles, the molecular polarizability is, therefore,

$$\alpha_m = \frac{3}{4\pi N_m} \frac{\varepsilon_1 - 1}{\varepsilon_1 + 2}. \tag{7}$$

Setting $\varepsilon_1 = 4.4$ and $N = 1.44 \times 10^{21}$ cm^{-3} (molecular density for solid C_{60}), we obtain $\alpha_m = 90$ Å^3 for the polarizability at $\omega = 10^5$ Hz. This value compares well with other determinations of the low-frequency molecular polarizability of C_{60}.[8]

We explain the dramatic increase in the dielectric function $\varepsilon_1(\omega)$ from 4.4 at 10^5 Hz to 18.4 at 100 Hz by the polarization caused by the interstitial oxygen. We determine the

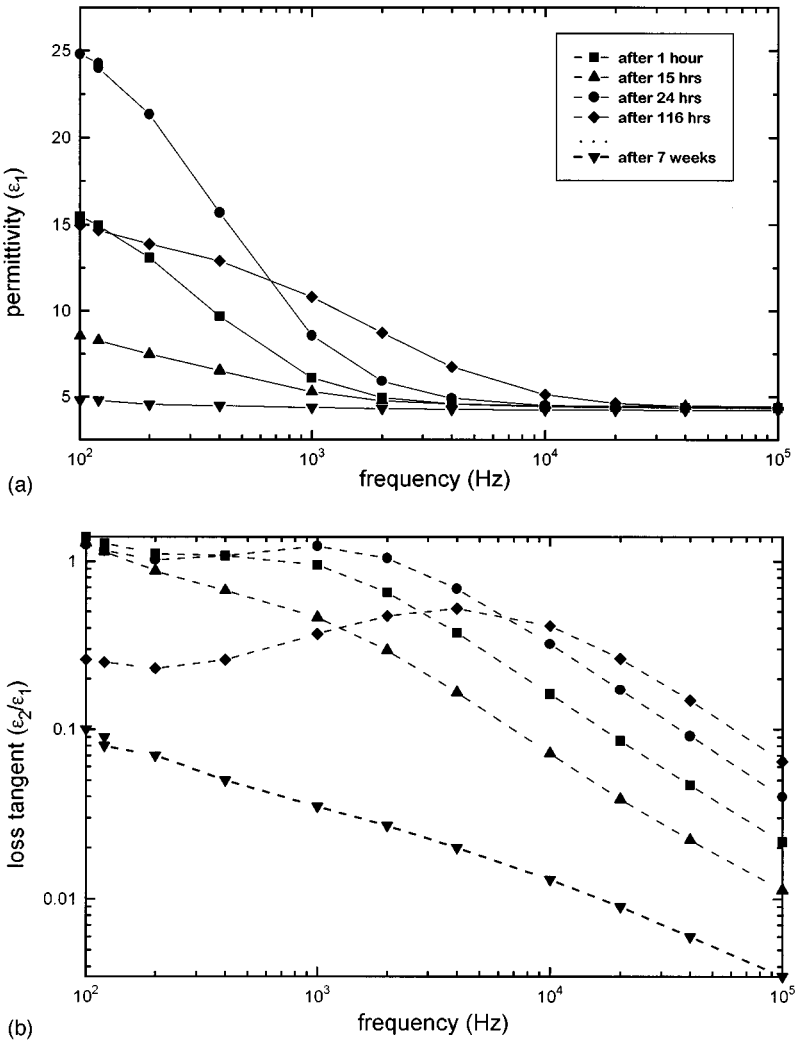

FIG. 7. Evolution of the dielectric properties of an oxygenated 857-Å-thick C_{60} film with exposure to the ambient atmosphere for various lengths of time. Note that, while the permittivity is plotted on a log-linear scale (a), the dielectric loss tangent is plotted on a log-log scale (b).

strength μ of a permanent dipole at room temperature by solving Eq. (6) with $\varepsilon = 18.4$, $\alpha_m = 90$ Å^3, and $T = 300$ K, which yields $\mu \approx 0.9$ D. We then represent each C_{60} molecule as a conducting sphere of radius $R \approx 5$ Å, and each oxygen molecule as a point-charge q transferring a fractional charge onto the C_{60} molecule (Fig. 8). From an image charge calculation (assuming that the charge that is being transferred to C_{60} is delocalized), we obtain the dipole moment

$$\mu = -qa\left[1 - \left(\frac{R}{a}\right)^3\right] \tag{8}$$

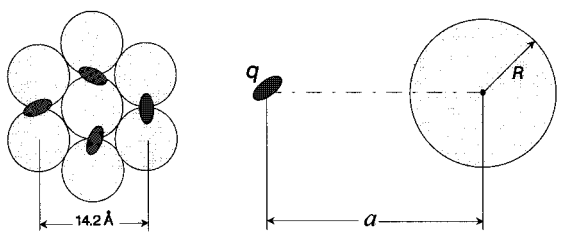

FIG. 8. A schematic drawing (two-dimensional projection) showing oxygen molecules (represented by ellipses) located in the interstitials of solid C_{60} (with C_{60} molecules represented by circles). The fcc C_{60} lattice constant is 14.2 Å. The figure to the right is used in the image charge calculation to obtain Eq. (8) for the dipole moment.

created by the transfer of a charge q onto a sphere of radius R located distance a from the charge q (see Fig. 8).

For the C_{60} solid with O_2 in the octahedral sites, $R \approx 5$ Å and $a \approx 7$ Å, and so q is determined to be

$$q \sim 0.04 q_{\bar{e}},$$

where $q_{\bar{e}} = 1.6 \times 10^{-19}$ C is the elementary charge on an electron. It is very plausible to expect this small amount of charge transfer to occur between a C_{60} molecule and an interstitial oxygen molecule through a hybridization mechanism. This validates our assumption regarding the origin of the dipoles in oxygenated C_{60}.

C. Diffusion-controlled relaxation mechanism

We explain the dynamics of the dielectric loss peak in terms of the oxygen diffusion and O_2-C_{60} charge transfer models described in Sec. IV B above. Since no oxygen is present in the as-prepared C_{60} film (see Fig. 7), no charge transfer occurs, and thus no dipoles are present. Therefore, no anomalous dielectric dispersion occurs in the as-prepared C_{60} film.

Once the sample is placed in the ambient environment, molecular oxygen starts diffusing into the bulk of the film, transferring charge to the neighboring C_{60} balls, and thus

creating electrical dipoles, as described in Sec. IV B. As the oxygen molecule diffuses through the C_{60} lattice, it ''drags'' this transferred charge from one C_{60} ball to the next along its path. Thus diffusion of an oxygen molecule through the lattice, which, on a microscopic level, is a random-walk-like process (see Sec. IV D), has the effect of flipping the O_2-C_{60} dipoles at some rate determined by the oxygen diffusion constant and the hopping distance. An applied ac electric field can couple to this process, yielding a loss peak at some frequency determined by the rate of oxygen hopping, which, in turn, is controlled by the diffusion constant of oxygen in its C_{60} host. We, therefore, propose a *diffusion-controlled relaxation* mechanism for low frequency dielectric relaxation in oxygenated C_{60}.

In the pristine C_{60} film, in the absence of a charge-transferring diffusant (such as O_2), no enhanced polarization [Fig. 7(a)] or anomalous dielectric dispersion [Fig. 7(b)] is expected. As a greater fraction of the interstitial sites is filled by diffusion, more dipoles are created via charge transfer, which results in increased polarization and the development of a dielectric loss peak at the characteristic hopping frequency of the molecules. As the number of empty sites decreases, oxygen molecules may need to hop to second-nearest-neighbor sites, which requires more energy, and is therefore much less likely to occur, resulting in a decrease in the additional polarization and in the magnitude of the loss peak. With further increased oxygenation, a nearly full occupancy of the interstitial sites is eventually achieved, interstitial hopping is inhibited, and the loss peaks, together with the enhanced polarization, disappear.

To exclude the possibility that the observed enhanced polarization behavior is due to some kind of an electrode effect, we also prepared trilayer structures qualitatively similar to those in Fig. 2, but with the electrodes made of metals other than aluminum (Ag, Au, and Cr). The invariance of the results with respect to variation of the electrode material appears to indicate that the enhanced polarization effects that we observe are due to intrinsic properties of the C_{60}-O_2 system, and not to electrode effects.

D. Obtaining the chemical and tracer diffusion constants from the dielectric loss data

There are two different diffusion constants that are often used in thermodynamics: a tracer diffusion constant $D_{\rm tr}$, and a chemical diffusion constant $D_{\rm ch}$ (see Fig. 9), the latter usually being simply designated as D. Our dielectric measurement techniques, spanning nine orders of magnitude in frequency, allowed us to obtain both of the constants simultaneously for the C_{60}-O_2 system, as discussed in this subsection.

Tracer diffusion is usually described as a random walk of the diffusing species (diffusant) in the lattice of the host material. The tracer diffusion constant is defined by the *Einstein relation*

$$D_{\rm tr}=\frac{\langle d^2\rangle}{2\tau}, \tag{9}$$

where d is the hopping distance, and τ represents the time required for a single *hop* in the random-walk chain.

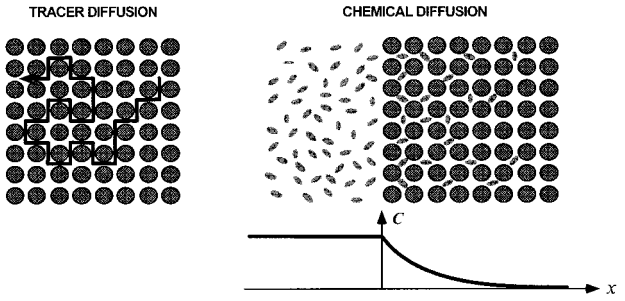

FIG. 9. Illustration of the tracer and chemical diffusion processes in two dimensions. The hollow circles represent atoms or molecules of the host material arranged in a regular lattice, into which the diffusant is diffusing. Tracer diffusion is a random walk-like process. The graph for the case of chemical diffusion shows a snapshot concentration of the material as a function of position x at some time t. The concentration C of the diffusant outside the sample is constant, and C decreases with x into the bulk of the material.

The *macroscopic* chemical diffusion constant $D_{\rm ch}$ describing the distribution of a diffusant in the host material is related to the *microscopic* tracer diffusion constant $D_{\rm tr}$ via the equation

$$D_{\rm ch}=FD_{\rm tr}, \tag{10}$$

where

$$F=\frac{C}{k_BT}\frac{\partial\mu}{\partial C}, \tag{11}$$

C is the diffusant concentration, and μ is the chemical potential. The distribution of a diffusant in a given film during absorption (or desorption) is governed by the one-dimensional diffusion equation (Fick's first law),[31] with the space coordinate x taken in the direction of the diffusion flux (see Fig. 9),

$$\frac{\partial C}{\partial t}=-\frac{\partial J}{\partial x}, \tag{12}$$

where $C(x,t)$ is the diffusant concentration, and J is the flux of the diffusant. Combining Fick's first law [Eq. (12)] with a differential mass balance equation

$$J=-D\frac{\partial C}{\partial x}, \tag{13}$$

where D is the (chemical) diffusion coefficient, we arrive at Fick's second law,

$$\frac{\partial C}{\partial t}=D\frac{\partial C^2}{\partial^2 x}+\frac{\partial D}{\partial C}\left(\frac{\partial C}{\partial x}\right)^2, \tag{14}$$

where the diffusion coefficient D may be a function of concentration C.

Solutions of Fick's second law [Eq. (14)] for various geometries and initial conditions were compiled by Crank.[32] For the case of lateral diffusion into the film of the kind expected in our Al-C_{60}-Al trilayer structures (see Fig. 2), the concentration of diffusant (e.g., molecular oxygen) at distance x into the film after time t is found to be[32]

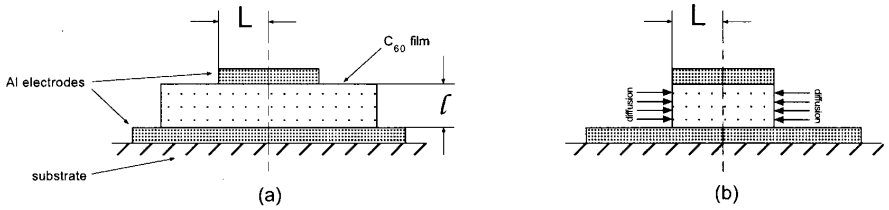

FIG. 10. Illustration of the approximations made in deriving the diffusion equations: (a) A single M-C_{60}-M (M is a metal) junction similar to those shown in Fig. 2, where ℓ represents the thickness of the C_{60} film, and L is one-half of the electrode width. (b) An approximation used in deriving Eqs. (15) and (16) assumes that the initial concentration is equal to C_1 across the C_{60} film's edges, and the diffusion of oxygen is into the C_{60} film. This approximation requires that $\ell \ll L$. For typical values of $\ell \sim 1000$ Å and $L \sim 100$ μm, this requirement is clearly fulfilled, and the use of this approximation is justified.

$$\frac{C(x,t)-C_0}{C_1-C_0}=1-\frac{4}{\pi}\sum_{n=0}^{\infty}\frac{(-1)^n}{2n+1}\cos(\alpha_n x)e^{-D\alpha_n^2 t}, \quad (15)$$

where C_0 is the initial diffusant concentration in the film (zero), C_1 is the concentration at the surface (saturated), D is the diffusion coefficient, $\alpha_n=(2n+1)\pi/(2L)$, and L is equal to one-half of the electrode width (see Fig. 10).

If $M(t)$ denotes the total amount of diffusing substance which has entered the film at time t, and M_∞ is the amount at equilibrium ($t\to\infty$), then the solution to Fick's second law can be written as[32]

$$\frac{M(t)}{M_\infty}=1-\frac{8}{\pi^2}\sum_{n=0}^{\infty}\frac{1}{(2n+1)^2}e^{-D\alpha_n^2 t}. \quad (16)$$

The value of t/L^2 for which $M(t)/M_\infty=\frac{1}{2}$, conveniently written as $t_{1/2}/L^2$, is given approximately by

$$\frac{t_{1/2}}{L^2}=-\frac{1}{\pi^2 D}\ln\left[\frac{\pi^2}{16}-\frac{1}{9}\left(\frac{\pi^2}{16}\right)^9\right], \quad (17)$$

the error being about 0.001% for typical values of the parameters.[33] Thus the approximation

$$D\simeq 0.05\left(\frac{L^2}{t_{1/2}}\right) \quad (18)$$

can be used so that if the half-time of the sorption process $t_{1/2}$ is observed experimentally, the value of the diffusion coefficient for a given temperature, assumed to be constant, can be determined.

In a remarkable illustration of the power and usefulness of dielectric measurements, we were able to measure both the tracer and chemical diffusion constants $D_{\rm tr}$ and $D_{\rm ch}$ of oxygen in C_{60} in a single measurement. Figure 11 displays the results of this measurement, plotting both the real $\varepsilon_1(f)$ and imaginary $\varepsilon_2(f)$ parts of the dielectric function over a broad frequency range. The measurements were performed on a 1000-Å-thick C_{60} film in the ''sandwich'' configuration (see Fig. 2). To map the dielectric function over nine decades in frequency, we had to utilize both the HP 4274A LCZ meter (for measurements from 100 Hz to 100 kHz) and the SI 1254 Frequency Response Analyzer (for measurements below 30 Hz), in configurations described in Sec. II. An additional preamplifier stage was necessary for measurements below 1 Hz, due to the increased effective conductivity of the sample at low frequencies. The excellent overlap of the data in the three measurement regions confirms the validity of our measurement techniques.

The Einstein relation [Eq. (9)] can be written in the frequency domain as

$$D_{\rm tr}=\frac{1}{2}\langle d\rangle^2 f_t, \quad (19)$$

where $\langle d\rangle\approx 7$ Å is the average oxygen molecule hopping length corresponding to the distance between two neighboring octahedral sites (see Fig. 8), and $f_t=1/\tau\approx 35$ Hz is the hopping frequency determined from the frequency of the dielectric loss peak in Fig. 11, yielding $D_{\rm tr}\approx 10^{-13}$ cm^2 s^{-1} using Eq. (19).

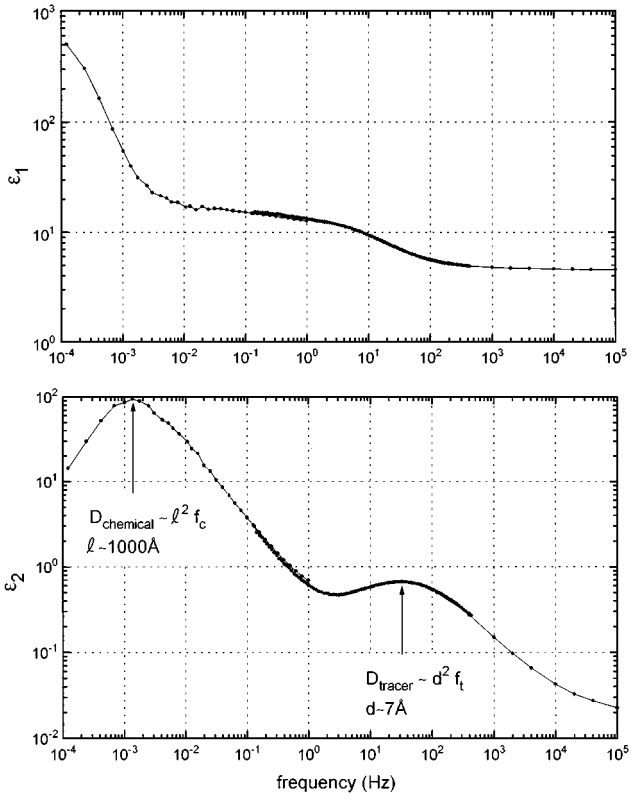

FIG. 11. Plot of the frequency dependent $\varepsilon_1(f)$ and $\varepsilon_2(f)$ used to determine the molecular oxygen diffusion into a C_{60} film. Peaks in $\varepsilon_2(f)$ due to both tracer and chemical diffusion processes are indicated.

To find the chemical diffusion coefficient $D_{\rm ch}$, we first note from Fig. 7 that the polarization and the dielectric loss both achieve their maximum values after $\sim$24 h of exposure to the ambient environment, corresponding to half-occupancy of the sites that are eventually occupied by oxygen, as described in Sec. IV C. This gives $t_{1/2}\sim 24$ h for the half-time of the sorption process of Eq. (18).

On the other hand, the same diffusion process that leads to the development and subsequent disappearance of the tracer diffusion (molecular hopping) dielectric loss peak in Fig. 7 should also show up as a ''relaxation'' of the interfacial polarization in the dielectric measurements. We can thus extend Eq. (18) to incorporate the chemical diffusion values obtained from dielectric measurements (Fig. 11),

$$D_{\rm ch}\approx 0.05\left(\frac{L^2}{t_{1/2}}\right)\approx \ell^2 f_c, \tag{20}$$

where f_c is the frequency position of the chemical diffusion-related loss peak in Fig. 11, corresponding to millihertz frequencies, and ℓ is the thickness of the C_{60} film (see Fig. 10). The origins of the chemical diffusion-related apparent polarization increase and the accompanying loss peak in Fig. 11 should be attributed to the interfacial polarization due to oxygen ions drifting back and forth between the plates of the capacitor under the very-low-frequency applied electric field. From Eq. (20), we estimate the chemical diffusion of molecular oxygen in C_{60} at room temperature to be within the margin of error from the tracer diffusion constant, i.e., $D_{\rm ch}\approx 10^{-13}\ {\rm cm}^2\ {\rm s}^{-1}$. (The variance in the results for $D_{\rm ch}$ obtained with the two methods presented in Eq. (20) is likely due to the different values of the diffusion coefficient in the lateral and normal directions of the sample.)

We have, therefore, demonstrated that the chemical diffusion constant can be determined by dielectric measurements either by following the evolution of the *tracer* diffusion (hopping) loss peak and detecting the half-time of the sorption process $t_{1/2}$, or by direct measurement of $f\sim 1/t_{1/2}$ via detecting the dielectric loss peak at very low frequencies due to *interfacial* polarization.

By making use of the Einstein relation connecting a charge carrier's diffusion constant D and its mobility μ,

$$\frac{\mu}{D}=\frac{q}{k_B T}, \tag{21}$$

we can estimate the mobility of oxygen molecules in the C_{60} film. Using $q\sim 0.04 q_e$ (as derived in Sec. IV B) and $T=300$ K, this molecular mobility is calculated to be $\mu_{O_2}\approx 10^{-13}\ {\rm cm}^2\ {\rm V}^{-1}\ {\rm s}^{-1}$, which is infinitesimal compared to carrier mobilities in C_{60} of 0.08–1 $\rm cm^2\ V^{-1}\ s^{-1}$ reported in the literature.[8] We, therefore, conclude that the contribution of diffusing oxygen ions to dc transport in C_{60} films is negligible.

E. Discussion

The oxygen-induced charge-transfer mechanism presented above explains very well the main features of the dielectric behavior of C_{60} films that we observe: (1) development of a low-frequency polarization increase accompanied by a dielectric loss peak; (2) evolution of this loss peak with increasing oxygen content; and (3) the eventual disappearance of the loss peak and additional polarization with full oxygenation of the specimen (once the majority of the interstitial lattice sites is occupied). In addition, there is ample evidence to support the proposition that oxygen does indeed diffuse into the interstitials of a fullerite (see Sec. IV A).

However, we should consider other possible sources of additional polarization, such as effects related to the interaction of C_{60} with the top and bottom Al interfaces in an Al-C_{60}-Al trilayer structure used in our dielectric measurements (Fig. 2).

Many authors[34–38] have shown charge transfer between Al and C_{60}. Similar charge transfer effects were found for other metals.[39–43] If we allow for the possibility of diffusion of metal atoms from the electrodes into the bulk of C_{60} (as some earlier studies[44,45] appear to indicate), then a charge-transfer mechanism similar to that developed for oxygen diffusion (Sec. IV B) would apply, resulting in a frequency-dependent polarization and a dielectric loss peak at low frequencies. One might then account for the peak's dynamics (similar to that described in Sec. IV C) by proposing that, as metal (e.g., Al) atoms oxidize, they become less mobile, which prevents them from hopping between adjacent C_{60} interstitials, thereby eliminating dielectric dispersion. It should be noted that all of our reasoning would apply to the interfacial metal diffusion-induced polarization in exactly the same way that it applies to the oxygen diffusion-induced effect. However, this scenario appears somewhat less than plausible, considering that, as shown in Sec. IV A, the dielectric peak observed in our films is reversible upon heat treatment ($T_{\rm HT}\simeq 200\ ^\circ$C) in vacuum. The strong metal-metal oxide (e.g., Al-Al_2O_3) bonds can hardly be expected to break easily at temperatures as low as 200°C.

V. TEMPERATURE DEPENDENCE OF THE DIELECTRIC FUNCTION IN OXYGENATED C_{60}

We measured the dielectric properties of C_{60} films (0.1 Hz$<f<$100 kHz) versus temperature (100 K$<T<$300 K). The results of this study are presented in Fig. 12. The highest-frequency dielectric loss peak in Fig. 12(b) corresponds to 290 K, and the loss peak moves down in frequency, as the temperature is lowered to 215 K in steps of 5 K. As demonstrated in Sec. IV A, the peaks that we observe are not Debye-like, as shown by the higher-frequency slope of $1-n=0.7$ (on the log scale) in the dielectric loss peak [Fig. 12(b)].

An Arrhenius plot of the frequency position of the dielectric loss peaks shown in Fig. 12(b) is presented in Fig. 13. We find that the peaks are indeed temperature activated with a functional dependence

$$f_p=f_0\exp\left(-\frac{E_\tau}{k_B T}\right), \tag{22}$$

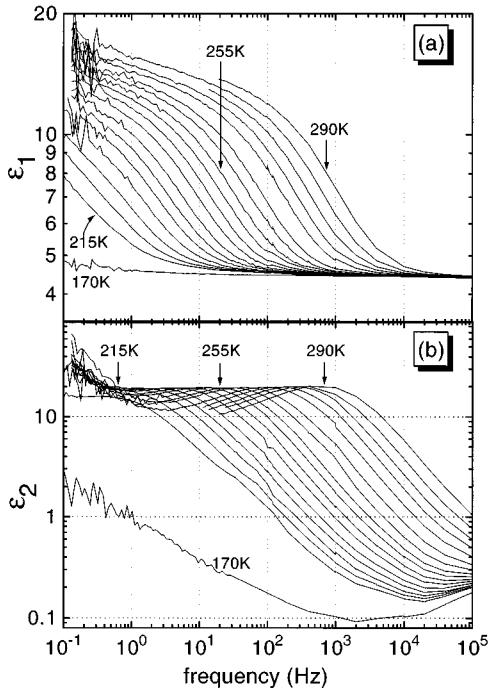

FIG. 12. Frequency dependence of the real (a) and imaginary (b) parts of the dielectric function of a 840-Å-thick C_{60} film plotted on a log-log scale for temperatures 215–290 K in 5-K intervals. The loss (ε_2) peak is activated with a $E_\sigma = 0.5$ eV energy barrier and a frequency prefactor of 2×10^{12} Hz (as found from the Arrhenius plot in Fig. 13). The loss peak in the ε_2 vs ω plot is not Debye-like, as shown by the higher-frequency slope of −0.7 (on the log scale), indicative of a correlated system. The broad increase in the loss function beyond 100 kHz for the low-temperature $\varepsilon_2(\omega)$ traces is due to residual rotations of C_{60} molecules below the $T_{01}\approx260$ K structural ''freeze-out'' transition. The hopping of the oxygen molecules also freezes out below ~190 K, resulting in a decrease of the slope of the dielectric loss (ε_2) and in a leveling off of the polarization (ε_1).

where E_τ is the activation energy, and f_0 is the frequency prefactor. From Fig. 13 we find that the activation energy of the loss peak below the phase transition at $T_{01}=260$ K is 0.35 eV whereas the activation energy above the phase transition is 0.49 eV, with a frequency prefactor $f_0=2\times10^{12}$ Hz comparable to the phonon frequencies.

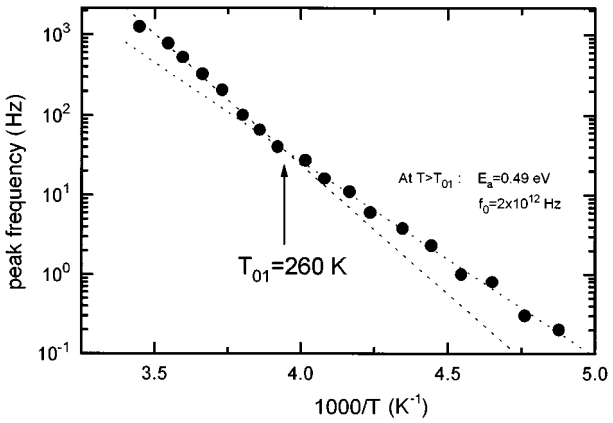

FIG. 13. Arrhenius plot of the position of the (tracer) dielectric loss peak frequency shown in Fig. 12(b).

Let us now return to Fig. 12 and consider the dielectric behavior of our system below the C_{60} structural transition at $T_{01}\approx260$ K. At temperatures below the T_{01} transition, theC_{60} molecules are not free to rotate any more and the loss peaks associated with their rotational motion [$\omega_{\rm rot}\sim10^9$ Hz at $T\sim300$ K (Ref. 9)] are moving into our frequency range [$\omega_{\rm rot}\sim10^5$–10^6 Hz at $T\sim160$ K (Refs. 10 and 46)] and appear as a broad increase in the loss function above 100 kHz. Below ~190 K the absolute value of the slope of the dielectric loss curve begins to decrease as well, reaching $n-1=0.37$ at 170 K [the bottom curve of Fig. 12(b)]. This shows that at low temperatures the hopping motion of the oxygen molecules freezes out, and the system becomes more strongly correlated, which, in turn, results in a leveling off of the polarization [see the bottom curve on Fig. 12(a), corresponding to the frequency response at 170 K].

VI. CONCLUSIONS

We used dielectric spectroscopy to measure the frequency and temperature dependence of the low-frequency dielectric function $\varepsilon(\omega)$ of thin C_{60} films. In order to explain the dielectric loss peak and the accompanying increase in polarization observed at ~10–100 Hz, a small charge transfer is inferred between the C_{60} and O_2 molecules which occupy interstitial spaces of solid C_{60} exposed to oxygen (or ambient air). Due to the large size of the C_{60} molecules, this small charge transfer creates large dipole moments, which in turn are coupled to the applied ac electric field via a *diffusion-controlled relaxation* mechanism. These dipole moments are responsible for a large increase of permittivity ε_1 at low frequencies. With increasing oxygenation, the interstitial sites eventually become nearly fully occupied, interstitial hopping is inhibited, and the loss peaks, together with the enhanced polarizations, disappear.

We note that C_{60} can be thought of as a rather potent ''charge sponge.'' In M_3C_{60} (M is an alkali metal), this leads to novel superconducting compounds;[47] in thin-film $\{\text{Al-C}_{60}\}_n$ multilayer structures, charge transfer leads to interesting interface effects;[34] and in our study, this charge transfer leads to an extraordinary additional polarization effect.

We conclude that dielectric spectroscopy can be used to assess the content of oxygen in the interstitial spaces of C_{60} solid. Both tracer and chemical diffusion coefficients can be determined for the same sample. We have used this technique in other work[12] to ascertain the effect of various intercalants on the dielectric properties of C_{60} films.

ACKNOWLEDGMENTS

We are pleased to acknowledge helpful discussions with Professor S. D. Senturia of MIT, Dr. R. C. Haddon of Bell Laboratories, and Dr. A. Hunt of the University of California at Riverside. Assistance by Dr. Huan Lee of Micromet Instrument is greatly appreciated. B.P. and M.S.D. would also like to acknowledge support by NSF Grant No. DMR 95-10093.

*Present address: University of Florida, Physics Department, Gainesville, FL 32611-8440.
[1] W. Kratschmer, L. D. Lamb, K. Fostiropoulos, and D. R. Huffman, Nature (London) **347**, 354 (1990).
[2] A. F. Hebard, R. C. Haddon, R. M. Fleming, and A. R. Kortan, Appl. Phys. Lett. **59**, 2109 (1991).
[3] G. B. Alers, B. Golding, A. R. Kortan, R. C. Haddon, and F. A. Theil, Science **257**, 511 (1992).
[4] S. L. Ren, Y. Wang, A. M. Rao, E. McRae, J. M. Holden, T. Hager, K. Wang, W.-T. Lee, H. F. Ni, J. P. Selegue, and P. C. Eklund, Appl. Phys. Lett. **59**, 2678 (1991).
[5] Y. Wang, J. M. Holden, A. M. Rao, W. T. Lee, X. X. Bi, S. L. Ren, G. W. Lehman, G. T. Hager, and P. C. Eklund, Phys. Rev. B **45**, 14 396 (1992).
[6] A. M. Rao, P. Zhou, K. A. Wang, G. T. Hager, J. M. Holden, Y. Wang, W.-T. Lee, X.-X. Bi, P. C. Eklund, D. S. Cornett, M. A. Duncan, and I. J. Amster, Science **259**, 955 (1993).
[7] E. Sohmen, J. Fink, and W. Krätschmer, Z. Phys. B Condens. Matter **86**, 87 (1992).
[8] M. S. Dresselhaus, G. Dresselhaus, and P. C. Eklund, *Science of Fullerenes and Carbon Nanotubes* (Academic, New York, 1996).
[9] C. S. Yannoni, R. D. Johnson, G. Meijer, D. S. Bethune, and J. R. Salem, J. Phys. Chem. **95**, 9 (1991).
[10] X. D. Shi, A. R. Kortan, J. M. Williams, A. M. Kini, B. M. Savall, and P. M. Chaikin, Phys. Rev. Lett. **68**, 827 (1992).
[11] A. K. Jonscher, *Dielectric Relaxation in Solids* (Chelsea Dielectrics, London, 1983).
[12] B. Pevzner, Master's thesis, Massachusetts Institute of Technology, Cambridge, MA, 1995.
[13] S. D. Senturia, Jr., N. F. Sheppard, H. L. Lee, and D. R. Day, J. Adhesion **15**, 69 (1982).
[14] N. F. Sheppard, D. R. Day, H. L. Lee, and S. D. Senturia, Sensors Actuators **2**, 263 (1982).
[15] S. D. Senturia and S. L. Garverick, U.S. Patent No. 4,423,371 (27 Dec. 1983).
[16] R. A. Assink, J. E. Schirber, D. A. Loy, B. Morosin, and G. A. Carlson, J. Mater. Res. **7**, 2136 (1992).
[17] C. C. Eloi, J. D. Robertson, A. M. Rao, P. Zhou, K-A. Wang, and P. C. Eklund, J. Mater. Res. **8**, 3085 (1993).
[18] T. Arai, Y. Murakami, H. Suematsu, K. Kikuchi, Y. Achiba, and I. Ikemoto, Solid State Commun. **84**, 827 (1992).
[19] C. Wen, J. Li, K. Kitazawa, T. Aida, I. Honma, H. Komiyama, and K. Yamada, Appl. Phys. Lett. **61**, 2162 (1992).
[20] P. M. He, Y. B. Xu, and X. J. Zhang *et al.*, J. Phys. Condens. Matter **5**, 7013 (1993).
[21] A. Zahab and L. Firlej, Solid State Commun. **87**, 893 (1993).
[22] D. Barančok, M. Haluška, V. Nádaždy, and J. Vajda, Solid State Commun. **94**, 597 (1995).
[23] J. Mort, R. Ziolo, M. Machonkin, D. R. Huffman, and M. I. Fegurson, Chem. Phys. Lett. **186**, 284 (1991).
[24] A. Hamed, Y. Y. Sun, Y. K. Tao, R. L. Meng, and P. H. Hor, Phys. Rev. B **47**, 10 873 (1993).
[25] J. Paloheimo, H. Isotalo, J. Kastner, and H. Kuzmany, Synth. Met. **56**, 3185 (1993).
[26] K. Hoshimono, S. Fujimori, S. Fujita, and S. Fujita, Jpn. Appl. Phys. Lett. **32**, L1070 (1993).
[27] N. Takahashi, H. Dock, N. Matsuzawa, and M. Ata, J. Appl. Phys. **74**, 5790 (1993).
[28] M. Hosoya, K. Ichimura, Z. H. Wang, G. Dresselhaus, M. S. Dresselhaus, and P. C. Eklund, Phys. Rev. B **49**, 4981 (1994).
[29] S. Fujimori, K. Hoshimono, and S. Fujita *et al.*, Solid State Commun. **89**, 437 (1994).
[30] R. C. Weast, *CRC Handbook of Chemistry and Physics* (CRC Press, West Palm Beach, FL, 1992).
[31] A. Fick, Ann. Phys. **170**, 59 (1855).
[32] J. Crank, *The Mathematics of Diffusion*, 2nd ed., (Oxford University Press, Oxford, 1975).
[33] B. S. Lim, A. S. Nowick, K.-W. Lee, and A. Viehbeck, J. Polym. Sci. **31**, 545 (1993).
[34] A. F. Hebard, C. B. Eom, Y. Iwasa, K. B. Lyons, G. A. Thomas, D. H. Rapkine, R. M. Fleming, R. C. Haddon, J. M. Phillips, J. H. Marshall, and R. H. Eick, Phys. Rev. B **50**, 17 740 (1994).
[35] H. Yonehara and C. Pac, Appl. Phys. Lett. **61**, 575 (1992).
[36] C. H. Lee, G. Yu, D. Moses, A. J. Heeger, and V. I. Srdanov, Appl. Phys. Lett. **65**, 664 (1994).
[37] A. V. Hamza, J. Dykes, W. D. Mosley, L. Dinh, and M. Balooch, Surf. Sci. **318**, 368 (1994).
[38] D. W. Owens, C. M. Aldao, D. M. Poirier, and J. H. Weaver, Phys. Rev. B **51**, 17 068 (1995).
[39] S. J. Chase, W. S. Bacsa, M. G. Mitch, L. J. Pilione, and J. S. Lannin, Phys. Rev. B **46**, 7873 (1992).
[40] Y. Kuk, D. K. Kim, Y. D. Suh, K. H. Park, H. P. Noh, S. J. Oh, and S. K. Kim, Phys. Rev. Lett. **70**, 1948 (1993).
[41] T. Hashizume, K. Motai, X. D. Wang, H. Shinohara, Y. Saito, Y. Maruyama, K. Ohno, Y. Kawazoe, Y. Nishina, H. W. Pickering, Y. Kuk, and T. Sakurai, Phys. Rev. Lett. **71**, 2959 (1993).
[42] E. I. Altman and R. J. Colton, Surf. Sci. **279**, 49 (1992).
[43] E. I. Altman and R. J. Colton, Surf. Sci. **295**, 13 (1993).
[44] D. Sarkar and N. J. Halas, Appl. Phys. Lett. **63**, 2438 (1993).
[45] R. L. McNally, F. R. Brotzen, A. J. Griffin, Jr., P. J. Loos, and E. V. Barrera, in *Novel Forms of Carbon II*, edited by C. L. Renschler, D. M. Cox, J. J. Pouch, and Y. Achiba, MRS Symposia Proceedings No. 349 (Materials Research Society, Pittsburgh, 1994), p. 205.
[46] R. Tycko, G. Dabbagh, R. M. Fleming, R. C. Haddon, A. V. Makhija, and S. M. Zahurak, Phys. Rev. Lett. **67**, 1886 (1991).
[47] A. F. Hebard, M. J. Rosseinsky, R. C. Haddon, D. W. Murphy, S. H. Glarum, T. T. M. Palstra, A. P. Ramirez, and A. R. Kortan, Nature (London) **350**, 600 (1991).